Model Analysis on the Performance for an Inertial Aided FLL-Assisted-PLL Carrier-Tracking Loop in the Presence of Ionospheric Scintillation

Tsung-Yu Chiou
Stanford University, Palo Alto, California

Demoz Gebre-Egziabher
University of Minnesota, Twin Cities, Minneapolis, Minnesota

Todd Walter and Per Enge
Stanford University, Palo Alto, California

BIOGRAPHY

Tsung-Yu Chiou is a Ph.D. candidate in the Aeronautics and Astronautics Department at Stanford University. He received his B.S. in Aerospace Engineering in 1998 from Tamkang University, Taiwan and his M.S. from Stanford in 2002. His research currently focuses on the performance analysis and validation of Inertial-aided GPS carrier-tracking loops. He is also looking into the solutions to the problem of GPS/WAAS performance degradation caused by ionospheric scintillation.

Dr. Demoz Gebre-Egziabher is an assistant professor of Aerospace Engineering and Mechanics at the University of Minnesota, Twin Cities. His research interests are in the areas of navigation and guidance. He was a member of the GPS Laboratory at Stanford University where he received a Ph.D. in Aeronautics and Astronautics.

Dr. Todd Walter received his B. S. in physics from Rensselaer Polytechnic Institute and his Ph.D. in 1993 from Stanford University. He is currently a Senior Research Engineer at Stanford University. He is a co-chair of the WAAS Integrity Performance Panel (WIPP) that focuses on the implementation of WAAS and the development of its later stages. Key contributions include: early prototype development proving the feasibility of WAAS, significant contribution to MOPS design and validation, co-editing of the Institute of Navigation's book of papers about WAAS and its European and Japanese counterparts, and design of ionospheric algorithms for WAAS. He was the co-recipient of the 2001 ION early achievement award.

Dr. Per Enge is a Professor of Aeronautics and Astronautics at Stanford University, where he is the Kleiner-Perkins, Mayfield, Sequoia Capital Professor in the School of Engineering. He directs the GPS Research Laboratory, which develops satellite navigation systems based on the Global Positioning System (GPS). These navigation systems augment GPS to improve accuracy and provide real time error bounds. Professor Enge's research focuses on the design of navigation systems which satisfy stringent requirements with respect to accuracy, integrity (truthfulness), time availability, and continuity. Enge has received the Kepler, Thurlow and Burka Awards from the Institute of Navigation (ION) for his work. He is also a Fellow of the ION and the Institute of Electrical and Electronics Engineers (IEEE). He received his PhD from the University of Illinois in 1983, where he designed a direct-sequence multiple-access communication system that provided an orthogonal signal set to each user.

ABSTRACT

Ionospheric scintillation has a significant impact on the availability of Global Positioning System (GPS) and Wide Area Augmentation System (WAAS), especially when the GPS/WAAS receiver is dynamically stressed. An example of such a scenario would be an aircraft using WAAS to make an approach and landing. This study investigated the tolerable wideband interference level given various conditions of ionospheric scintillation. Two important criteria are used to determine the tolerable

wideband interference level: the tracking threshold and the word error rate (WER) of the navigation data demodulation. An inertial aided FLL-assisted-PLL carrier-tracking loop is considered to be effective for increasing the receiver robustness to interference. This paper quantitatively gives the improvement using the inertial aided FLL-assisted-PLL and compares it to the generic PLL as well as inertial aided PLL carrier-tracking loops. Theoretical model analysis was performed for the above three tracking-loop configurations considering all possible error sources which can potentially degrade carrier-tracking loop performance. These errors include satellite/receiver clock dynamics, platform dynamics, platform vibrations, sensitivity of the receiver clock to acceleration, wideband interference, and ionospheric scintillation. The results showed that there is a 10 dB improvement in the minimum C/N_0 by using a FLL as a backup tracking loop when compared to the receiver with PLL used as the primary tracking loop only. However, satisfying the requirements of the WER limits the performance of this technique.

Key words: Phase-Locked Loop (PLL), Frequency-Locked Loop (FLL), Ionospheric Scintillation

I. INTRODUCTION

The application of GPS and WAAS in aviation has become very important since the first operation of WAAS in 2003. The signals received at an airplane have traveled through the atmosphere's layer from the satellites in orbits. As a result, the transmitted signals have been degraded by several uncertainties. One of the largest channel errors is due to the perturbations imposed by the ionosphere layer. This channel degradation caused by ionosphere can be divided in two categories. The first ionosphere error is the nominal ionosphere delay, which can be predicted by the Klobuchar model or be well removed by a dual frequency technique. The second ionosphere error is known as ionospheric scintillation. Ionospheric scintillation is caused by local ionosphere plasma anomalies. A deep signal power fading and rapid phase variations are the typical characteristics made by ionospheric scintillation. Either the power fading or the phase variations may lead to loss of signal lock or increases in measurement errors. As a result, the happen of ionospheric scintillation is a continuity threat to WAAS. The impacts of ionospheric scintillation on the GPS/WAAS receiver used for an aviation application shown in Figure 1 are of the interest in this work. Furthermore, robustness of the carrier tracking loops is indeed the key issue in the evaluation of the GPS/WAAS receiver performance under ionospheric scintillation.

To evaluate the robustness of the tracking loops to ionospheric scintillation, both of the errors due to scintillation and the generic tracking loop errors must be considered. Previous work in this area, in general, can be divided in two groups. In the first group, a number of researchers have studied the effects of ionospheric scintillation on tracking loop performance [1 to 6]. A very exhaustive research effort was made by Knight [1] to evaluate ionospheric scintillation effects on GPS receivers. In addition to the linear model approach, an intensive hardware testing has been conducted by Morrissey and et al [7, 8, and 9]. The second group of the previous researchers contributed to determine the tracking loop performance without considering ionospheric scintillation [11 to 17]. In particular, most attentions in the previous work were on a phase-locked loop (PLL). Relatively few studies have been done on a frequency-locked loop (FLL). Except that in [18 and 21], the use of a FLL to assist to a PLL was studied. A comprehensive FLL linear model study on the noise performance with different frequency discriminators was conducted in [19 and 20]. Recently, in [22 and 23], the FLL linear model including various error sources were considered. The use of a FLL to cope with ionospheric scintillation was implemented to process simulated scintillation data in [10]. It was demonstrated in [10] that a FLL is effective for the cycle slip detecting under scintillation environments.

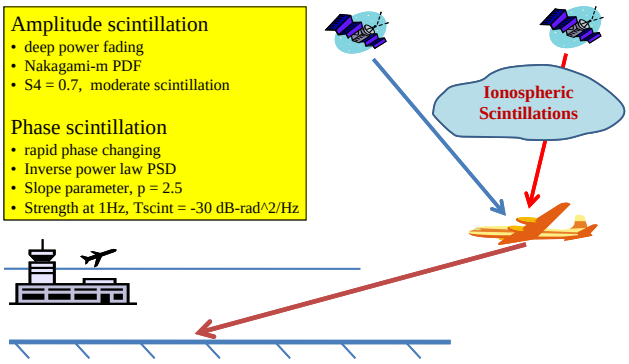

Figure 1: Problem Statement

Although much work has been done on the impacts of scintillation on a PLL, little attention has been paid to using a FLL to treat scintillation problems. As will be seen in this paper, a FLL is more robust to noise and dynamics compared to a PLL. However, a FLL provides more noisy measurements than a PLL does. An effective aiding scheme is considered to take the advantages of a FLL but without suffering from the noisy measurements provided by the FLL. The benefits of using an inertial aided carrier tracking loop on dealing with ionospheric scintillation has not been investigated either.

In this research, we attempt to provide an inclusive linear model analysis on both of PLL and FLL by considering all of the generic tracking error sources as well as the errors due to ionospheric scintillation. The purpose is to determine whether the use of a FLL as a backup tracking loop could effectively to cope with ionospheric scintillation. To examine the benefits of the technique of inertial aided FLL-assisted PLL, we aimed to determine the lowest tolerable signal power to noise power density ratio (C/N_0) with the following requirements satisfied for both GPS and WAAS signals. **First, the phase estimate error from a PLL must be smaller than a defined tracking threshold. Second, the frequency estimate error from a FLL must be less than a defined tracking threshold. Finally, the WER, by using either a PLL or a FLL, for both GPS (30 bits) and WAAS (250 bits) must be less than 10^-4 required by [24]**.

A basic understanding of generic GPS/WAAS receivers is crucial before moving on to the specifics of linear models of tracking loops.

II. ARCHITECTURE OF A GPS/WAAS RECEIVER

This section will provide a brief overview of a GPS/WAAS receiver. Figure 2 shows a GPS/WAAS receiver block diagram [page 432, 25]. The transmitted L-band GPS/WAAS signals are captured by the antenna. A signal conditioning process is done by the front-end to down-convert the signals from radio frequency (RF) to an appropriate intermediate frequency (IF) such that the acquisition and tracking are applicable in the next step. The operation of the tracking loop for GPS and WAAS is the same except that the maximum coherent integration time for WAAS is only one tenth of GPS's because the symbol rate for WAAS is 500 symbols per second but for GPS is 30 bits per second. So, the demodulation process is where really differentiates the WAAS signals from the GPS signals. An extra convolutional encoding has been applied on the WAAS message. Therefore, an extra decoding step must be added, such as Viterbi decoding [42], to extract the final 250 bits of WAAS messages. At the step of demodulation, a binary phase shift keying (BPSK) demodulation is used if the carrier tracking loop is a PLL. By contrast, if a FLL is used for the carrier tracking loop, a differential phase shift keying (DPSK) demodulation is needed [20 and page 381 of 26]. The details of this DPSK scheme will be discussed in Section VI. The current focus of the coming sections is to discuss the carrier tracking loop. The carrier tracking loop can be a stand alone PLL, an inertial aided PLL, a stand alone FLL, and an inertial aided FLL. However, a simple FLL aiding the traditional PLL tracking loop is considered to be effective to the problem caused by ionospheric scintillation.

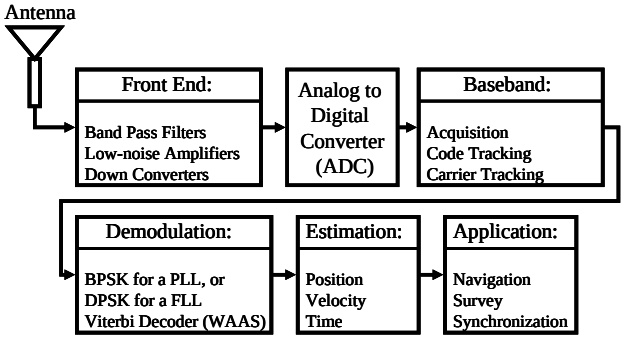

Figure 2: Block Diagram of a GPS/WAAS Receiver

III. FLL AIDING SCHEME

From the thermal noise performance analysis [20, 26], a FLL is more robust to noise than a PLL. Moreover, a FLL can tolerate higher platform dynamics as well as clock dynamics [27]. Therefore, to combine the best of both, the technique called FLL-assisted-PLL was introduced in [21]. In [21], the carrier tracking loop fused the FLL tracking to the PLL tracking. Both types of tracking loop operate in parallel. The overall performance of this fused FLL-assisted-PLL is between a stand alone FLL and a stand alone PLL. In our opinion, it is not desirable to operate a FLL as the carrier tracking loop for long term since the frequency estimate is noisy. Also the probability of losing lock of a FLL increases as time goes on. Hence, using a FLL as a backup tracking loop is considered in this paper. The FLL is used in a short period of time when the C/N_0 is low. In fact, the power fading caused by amplitude scintillation is indeed this type of problem.

Figure 3 shows the FLL aiding scheme which is considered to be effective to cope with the tracking challenge imposed by amplitude scintillation. The basic idea depicted in Figure 3 is to use the FLL as a backup tracking loop, which was also proposed in [22]. In nominal conditions, C/N_0 of GPS or WAAS signals is usually above the tracking threshold of a PLL with appropriate noise bandwidth. However, in the presence of amplitude scintillation, C/N_0 will suddenly drop below the tracking threshold of the PLL. As a result, the PLL may have cycle clips or even lose lock on the signal. However, fortunately, a deep power fading usually stands a very short period amount of time (Dt). During this brief moment of deep power fading, the receiver takes the frequency estimate from the FLL instead of the phase estimate from the PLL since the PLL is no longer to be able to provide reliable measurements. When C/N_0 is recovered back to the nominal condition, the receiver will switch back to the PLL. In this aiding scheme, the FLL

has to be reinitialized when C/N_0 is high because the probability of losing lock of the FLL increases with time. The time (T_{ini}) to reinitialize the FLL limits the lower bound of the noise bandwidth of the FLL. Since a FLL with smaller noise bandwidth has a longer time constant, T_{ini} has to be at least one time constant of the FLL such that any transient responses converge. Given this FLL aiding scheme, we are ready to evaluate the performance of carrier tracking loops.

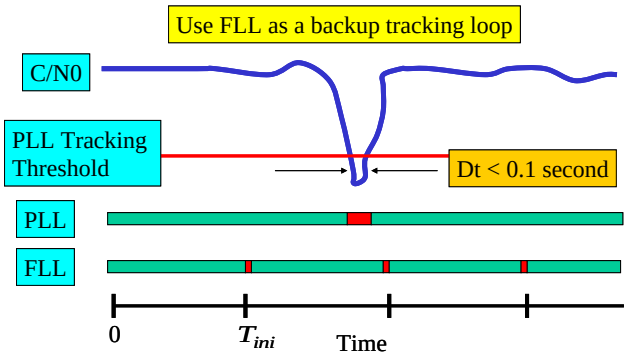

Figure 3: FLL Aiding Scheme

IV. MODELS OF SCINTILLATION

As mentioned, ionospheric scintillation can be decomposed into two components: phase scintillation and amplitude scintillation. They are defined by their power spectral densities (PSD) and probability density functions (PDF). In this section, we simply review the mathematical models of the said PSD's and PDF's. Characterizing the model of ionospheric scintillation is not the purpose of this work. The focus of this paper is to evaluate the improvement by using an inertial aided PLL or FLL given the PSD's and PDF's of scintillation.

The PSD of phase scintillation follows an inverse power law, which is given in the flowing form [28]:

$$S_{\delta\phi_p}(f) = \frac{T_{sct}}{\left(f_0^2 + f^2\right)^{p/2}}, \quad radians^2/Hz \qquad (1)$$

where T_{sct} is the magnitude of the PSD at the frequency of 1 Hz, f is the frequency of phase fluctuations, f_0 is the frequency corresponding to the maximum irregularity size in the ionosphere, and p is the slope of the PSD (usually in the range 1 to 4 and typically 2.5). In this paper, we pick the typical values for the constants in Eq. (1). $T_{sct} = -30 \ \ dB-radians^2$, $f_0 = 1e-4 \approx 0$, and $p = 2.5$ [1].

Before defining the PDF of amplitude scintillation, an important parameter, S_4 , describing the strength of amplitude scintillation has to be defined. S_4, the intensity scintillation index, is the normalized root mean square (RMS) intensity and is given by [page 45 of 1, 9]

$$S_4 = \sqrt{\frac{\left\langle I^2 \right\rangle - \left\langle I \right\rangle^2}{\left\langle I \right\rangle^2}}, \qquad (2)$$

where I is the signal intensity, and $\langle \bullet \rangle$ is the expectation operator.

The PDF of amplitude scintillation is modeled as a Nakagami-m distribution, which is given by [29]

$$f_A(A) = \frac{2m^m A^{2m-1}}{\Gamma(m)\left\langle A^2 \right\rangle^m} e^{-mA^2/\left\langle A^2 \right\rangle}, \quad A \geq 0 \qquad (3)$$

where A is the signal amplitude, $\Gamma(\bullet)$ is the Gamma function and m is defined as $m = 1/S_4^2$. Given the mean square amplitude, $\left\langle A^2 \right\rangle$, and the m parameter, the Nakagami-m distribution for amplitude scintillation is well defined. In this paper, S_4 is set to be 0.7, which represents a moderate scintillation [5]. Given the PSD in Eq. (1), using a linear model analysis can determine the estimated phase (in PLL) or frequency (in FLL) variance caused by phase scintillation. The estimated phase or frequency variance caused by amplitude scintillation will be shown in a combined form with the noise performance of a carrier tracking loop. The PDF of amplitude scintillation will be used to determine the bit error rate (BER) when the received signals are corrupted by amplitude scintillation.

Thus far, the error sources from scintillation have been described. In the following two sections, the PLL linear model analysis and FLL linear model analysis will be provided, respectively.

V. PHASE-LOCKED LOOP (PLL) LINEAR MODEL ANALYSIS

In this section, a PLL linear model analysis will be discussed. A very comprehensive discussion on the generic linear model analysis has been done in [12] and no intention exists to duplicate their analysis here. For more details, [12] is highly recommended for further readings. Instead, we attempted to address those error sources, which were not covered previously. Also of interest to us is the improvement on the carrier tracking

loop performance by using a very low acceleration sensitivity oscillator. Likewise, providing the fundamental framework on the PLL linear model analysis would be helpful on the understanding for the FLL analysis in the coming section. However, we will only discuss every error source to the PLL without details.

A short discussion on the functions of a PLL was given in [16]. Here we started with a PLL linear analysis. To analyze the phase error of a PLL, a linear model illustrated in Figure 4 is considered. The input φ_i is the phase of the incoming digital IF signal. The output φ_o is the phase steered by the PLL to track the input φ_i. The summation symbol in Figure 4 represents the phase discriminator. Thus, $\delta\varphi$ is the phase error between φ_i and φ_o. $G(s)$ is the plant of the closed-loop, which is the object to be controlled. For the PLL shown here, $G(s)$ is also called a the numerically controlled oscillator (NCO). Therefore, $G(s)$ represents a pure integrator, which can be written as $1/s$. $F(s)$ is the controller, where we design the parameters to control the bandwidth of the overall closed-loop. Ideally, $\delta\varphi$ stays exactly at zero once the phase is locked in. However, the incoming phase signal φ_i is influenced by the thermal noise, the dynamics of the platform, ionospheric scintillation, and even the satellite clock dynamics. Furthermore, the replica carrier phase φ_o is affected by the receiver clock dynamics and an extra phase instability induced by the platform vibration. As a result, the phase error source includes the thermal noise, platform dynamics stress error, receiver and satellite clock dynamics, and the oscillator's frequency error induced by the platform vibrations.

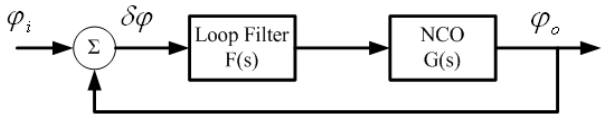

Figure 4: PLL Linear Model

A higher bandwidth PLL has better performance to track the dynamics. However, a higher bandwidth PLL has poor capability on noise suppression. Therefore, the phase error response is a parameter for judging a proper PLL bandwidth. Specifically, the standard deviation value (1-sigma) of the steady state phase error is used as a metric to characterize the performance of the PLL alone or the inertially-aided PLL. The 1-sigma phase error is also called phase jitter [27], which is represented by

$$\sigma_{\delta\rho} = \sqrt{\sigma_{\delta\rho\omega}^2 + \sigma_{\delta\rho sv}^2 + \sigma_{\delta\rho rx}^2 + \sigma_{\delta\rho v}^2 + \sigma_{\delta\rho p}^2} + \frac{\theta_e + \theta_{acc}}{3}, \quad \text{radians} \tag{4}$$

where

$\sigma_{\delta\rho\omega}$ = phase jitter from thermal noise and amplitude scintillation (if applied);

$\sigma_{\delta\rho sv}$ = phase jitter from the instability of the satellite's oscillators;

$\sigma_{\delta\rho rx}$ = phase jitter from the instability of the receiver's oscillators;

$\sigma_{\delta\rho v}$ = the vibration induced phase jitter;

$\sigma_{\delta\rho p}$ = phase jitter caused by phase scintillation;

θ_e = dynamic stress in the PLL tracking loop

θ_{acc} = the excessive bias phase error induced by the acceleration sensitivity of the local oscillator.

In general, the phase jitter of a PLL can be evaluated by

$$\sigma_{\delta\varphi}^2 = \int_0^\infty (|H(j2\pi f)|^2 S_\omega(f) + |1 - H(j2\pi f)|^2 S_{\delta\phi}(f)) df, \tag{5}$$

where $H(j2\pi f)$ is the closed-loop transfer function of the linear model shown in Figure 4, $S_\omega(f)$ is the power spectral density of the phase noise from thermal noise or amplitude scintillation, and $S_{\delta\phi}(f)$ is the power spectral density of the additional phase noise from satellite and receiver oscillators or phase scintillation. By definition the closed-loop transfer function is written as follows

$$H(s) = \frac{\varphi_o}{\varphi_i} = \frac{G(s)F(s)}{1 + G(s)F(s)}. \tag{6}$$

It can be calculated that [16]

$$|1 - H(j2\pi f)|^2 = \frac{f^{2k}}{f_n^{2k} + f^{2k}}, \tag{7}$$

where k is the order of the closed-loop and f_n is the natural frequency of the closed loop in Hz.

Since the overall transfer function is a low pass filter, from Eq. (5), we can see that reducing the bandwidth of the loop would reject more thermal noise but unavoidably induce more phase error contributed by the additional phase noise due to oscillator's dynamics or phase scintillation. As a result, it is a convex problem. There is a minimum allowable one-sided noise bandwidth, B_n, such that the lowest tolerable C/N_0 is achieved.

In the rest of this section, the mathematical representation of each error source will be provided.

V-1. THERMAL NOISE AND AMPLITUDE SCINTILLATION ($\sigma_{\delta\rho\omega}$)

Thermal noise tracking error of a PLL with a dot-product phase discriminator in the presence of amplitude scintillation is derived in [page 105 of 1, and 30] and is given as follows

$$\sigma^2_{\delta\rho\omega} = \frac{B_n}{\frac{C}{N_0}(1-S_4^2)}\left[1+\frac{1}{2T_{coh}\frac{C}{N_0}(1-2S_4^2)}\right] \quad radians^2 , \tag{8}$$

where

B_n is the PLL one-sided noise bandwidth in Hz;

$\frac{C}{N_0}$ is the signal-to-noise power density ratio;

T_{coh} is the coherent integration time in second, 0.02s for GPS and 0.002s for WAAS;

$S_4 < 0.707$ for L1 signal.

If there is no amplitude scintillation, $S_4 = 0$, Eq. (8) becomes the standard thermal noise tracking error for the PLL [26]

$$\sigma^2_{\delta\rho\omega} = \frac{B_n}{\frac{C}{N_0}}\left[1+\frac{1}{2T_{coh}\frac{C}{N_0}}\right] \quad radians^2 . \tag{9}$$

V-2. RECEIVER OSCILLATOR PHASE NOISE ($\sigma_{\delta\rho rx}$)

The second phase error source is contributed by the receiver oscillator phase noise especially at a low noise bandwidth. One can increase the noise bandwidth such that the PLL can track the clock dynamics. However a higher noise bandwidth introduces more effects on the phase error caused by the thermal noise. To determine an appropriate noise bandwidth, we need to ascertain the carrier phase-noise spectrum. The phase-noise power spectral density (PSD) (one-sided) of an oscillator can be written as [31]

$$W_{\delta\phi rx}(f) = \sum_{i=-4}^{0} h_i f^i, \quad f_l \le f \le f_h. \quad radians^2/Hz \tag{10}$$

The lower bound of the frequency range, f_l, can be set to be 0 without losing any generalities [31]. The upper bond of the frequency range, f_h, can be very large but it will be limited by the pre-detection integration bandwidth (or coherent integration time) of the receiver. So, by definition, $f_h = 1/2T_{coh}$ in Hz. $W_{\delta\phi rx}(f)$ is the basband spectrum of the phase noise $\phi(t)$ [32], which is also known as the spectral density of the phase fluctuations [33]. It is important to note that $W_{\delta\phi rx}(f)$ is the PSD defined at the oscillator's center frequency, f_0. In fact, the actual phase noise PSD seen by the tracking loop should be the PSD at the received signal frequency, for example, GPS L1 frequency (f_{L1}). Define a multiplication factor between the received carrier frequency ($f_{carrier}$) and the local oscillator's center frequency (f_0) to be

$$N = \frac{f_{carrier}}{f_0} . \tag{11}$$

In this paper, $f_{carrier} = f_{L1}$. As a result, the phase noise PSD at the input of the carrier tracking loop should be

$$S_{\delta\phi rx}(f) = N^2 W_{\delta\phi rx}(f), \quad radians^2/Hz. \tag{12}$$

To illustrate this magnification effect on the phase noise, let us assume the oscillator's center frequency is 10.23 MHz. Therefore, N = 154 for L1 signal. The final phase noise PSD at f_{L1} is increased by $20\log_{10}(N) = 43.75$ dB from the original noise PSD at f_0. One should keep in mind that the phase noise PSD is defined at a specific center frequency.

In order to accomplish the analysis here, the coefficients h_i in Eq. (10) must be found for a given oscillator. However, what is given in the specification sheet of an oscillator is not the phase noise PSD defined in Eq. (10). The specification sheet usually gives the single-sideband (SSB) phase noise, $L(\Delta f)$, and it is usually expressed in decibel format as $10\log_{10}[L(\Delta f)]$ dBc/Hz [32, 33]. As stated in [32], "*dBc means "dB relative to carrier," where the term carrier actually means total power in the signal; "per Hz" refers to a bandwidth of 1 Hz.*" $L(\Delta f)$ is the normalized version of the theoretical passband spectrum of the oscillator signal [32]. A more concise definition of $L(\Delta f)$ given in [page 147, 32] depicted that "$L(\Delta f)$ *is the noise power, relative to the total power in the signal, in a bandwidth of 1 Hz in a single sideband at a frequency offset of* Δf *from the carrier frequency* f_0*.*"

The relationship between $W_{\delta\phi rx}(f)$ and $L(\Delta f)$ can be defined only if the following statement is true. The phase fluctuations at frequencies greater than the offset frequency are much less than 1 $radians^2$ [33]. In other words, if the phase-noise amplitude is small enough, it is shown that [35]

$$L(\Delta f) \approx \frac{W_{\delta\phi rx}(f)}{2}. \quad (13)$$

Through the relation in Eq. (13), we can find the coefficients, h_i, in Eq. (10) from the given SSB in the specification sheet of an oscillator. Table 1 shows the SSB of several types of oscillators and Table 2 shows the resolved coefficients, h_i, for $W_{\delta\phi rx}(f)$. However, as mentioned in [page 150, 32], *"the phase noise amplitude is never small enough at frequencies close in to the carrier frequency, so $W_{\delta\phi rx}(f)$ is never a good representation of the close-in $L(\Delta f)$, the close-in RF sidebands."* This discrepancy may not be pronounced since the process of the phase noise due to oscillators through the tracking is a high pass filtering process. The large discrepancies at low frequency range, i.e. close to the carrier frequency, will be filtered out. If the noise bandwidth of the tracking is really small (much less than 1 Hz), the imperfect phase noise model starts to degrade the results predicted by this analysis. Hence, the tracking error due to oscillator dynamics is an approximated result but it is the best solution one can obtain currently.

Given the PSD in Eq. (12), we can find the phase jitter from oscillator's dynamics by evaluating the second integrand in Eq. (5) as follows

$$\sigma^2_{\delta\phi rx} = \int_0^\infty \left|1 - H(j2\pi f)\right|^2 S_{\delta\phi rx}(f)df. \quad (14)$$

Substitute Eqs. (7) and (12) into Eq. (14), we obtained the phase jitter from oscillator's dynamics only in terms of the PLL noise bandwidth, B_n, as follows [16]

for a second order PLL ($k = 2$),

$$\sigma^2_{\delta\phi rx} = N^2[X^3 h_4 \frac{\pi}{2\sqrt{2}} + X^2 h_3 \frac{\pi}{4} + X h_2 \frac{\pi}{2\sqrt{2}}] \quad radians^2, \quad (15)$$

where $X = \frac{2\pi}{1.8856 B_n}$ and N was defined in Eq. (11);

and for a third order PLL ($k = 3$),

$$\sigma^2_{\delta\phi rx} = N^2[Y^3 h_4 \frac{\pi}{6} + Y^2 h_3 \frac{\pi}{3\sqrt{3}} + Y h_2 \frac{\pi}{3}] \quad radians^2, \quad (16)$$

where $Y = \frac{2\pi}{1.2 B_n}$ and N was defined in Eq. (11).

Note that the unit of B_n is Hz.

Table 1: Specifications of Oscillators

Oscillators \ SSB (dBc/Hz)	f0 (MHz)	Kg (ppb/G)	1 Hz	10 Hz	100 Hz	1 kHz	10 kHz
TCXO, Rakon IT5300B	16.3676	2	-57	-88	-112	-130	-140
OCXO, Agilent E4424B	10.0	1	-88	-118	-128	-135	-147
OCXO, ISOTEMP 91-1	10.0	1	-89	-120	-140	-151	-154
OCXO, Oscilloquartz 8607	10.0	0.5	-122	-137	-143	-145	-145
Rubidium, SRS PRS10	10.0	1	-103	-135	-150	-152	-153
Cesium, Typical Values [48, 49]	10.0	1	-105	-135	-160	-170	-190
OCXO, MTI 250L, low g-sensitivity	10.0	0.1	-90	-120	-140	-155	-160

Table 2: Coefficients of Oscillattor's PSD

Oscillators \ Coefficients	h0	h1	h2	h3	h4
TCXO, Rakon IT5300B	9.9e-15	9.1e-11	9.7e-8	2.0e-6	1.9e-6
OCXO, Agilent E4424B	1.8e-15	1.0e-11	1.2e-10	1.8e-11	2.8e-9
OCXO, ISOTEMP 91-1	7.2e-16	7.1e-13	1.6e-10	1.6e-10	2.2e-9
OCXO, Oscilloquartz 8607	6.4e-15	3.2e-13	2.2e-14	8.7e-13	3.9e-14
Rubidium, SRS PRS10	9.9e-16	9.6e-14	1.6e-15	4.7e-11	5.3e-11
Cesium, Typical Values	6.2e-19	1.4e-14	7.6e-23	6.2e-11	1.5e-12
OCXO, MTI 250L	1.8e-16	3.5e-13	1.6e-10	1.0e-10	1.7e-9

V-3. SATELLITE OSCILLATOR PHASE NOISE ($\sigma_{\delta\rho sv}$)

Other than the receiver oscillator on the earth that produces phase noise, the clock onboard in the orbit could also generate phase noise in the signals. The nominal satellite oscillator PSD was not available. However, it was promised that the phase jitter from satellite oscillator's dynamics is less than 0.1 radians when B_n is 10 Hz [34]. As shown in [12], this specification is somewhat conservative. We use a typical specification of a Cesium clock as given in Table 1 to model the satellite oscillator's dynamics. The expression for $\sigma_{\delta\rho sv}$ is the same as those in Eqs. (15) and (16) except that the coefficients, h_i, were taken from Table 2 for the Cesium clock.

V-4. VIBRATION INDUCED PHASE JITTER ($\sigma_{\delta\rho v}$)

The phase jitter induced by the platform vibration can be calculated by

$$\sigma^2_{\delta\varphi v} = \int_0^\infty |1 - H(j2\pi f)|^2 S_{\delta\phi v}(f) df \quad radians^2, \tag{17}$$

where $S_{\delta\phi v}(f)$ is the PSD of the phase noise induced by the platform vibrations. $S_{\delta\phi v}(f)$ can be further expressed as follows [26]

$$S_{\delta\phi v}(f) = (k_g N f_0)^2 \frac{G_g(f)}{f^2}, \tag{18}$$

where k_g is the oscillator's g-sensitivity in parts/g (values given in Table 1), f_0 is the center frequency of the oscillator (values given in Table 1), N has been defined in Eq. (11), and $G_g(f)$ is the one-sided vibration spectral density in g^2/Hz. The most up-to-date vibration spectral density curve for an instrument panel installation on a turbojet aircraft is shown in Figure 5 [36]. Figure 5 also shows a vibration spectrum of an automobile (sedan) in normal driving condition [14]. Table 3 summarizes the two curves in Figure 5. Eq. (17) was evaluated numerically in this work.

Table 3: Vibration PSDs

Aircraft (RTCA 160D)		Automobile	
Vibration PSD (g^2/Hz)	Frequency (Hz)	Vibration PSD (g^2/Hz)	Frequency (Hz)
3.0*10^-3	f < 40	2.0*10^-5	f < 0.5
(3.0*10^-3)*(f/40)^-2	40 < f < 100	2.0*10^-4	0.5 < f < 2.5
5.0*10^-4	100 < f < 500	2.0*10^-5	2.5 < f < 15
(5.0*10^-4)*(f/500)^-2	500 < f	2.0*10^-3	15 < f < 30
		(2.0*10^-5)*(f/30)^-6	30 < f

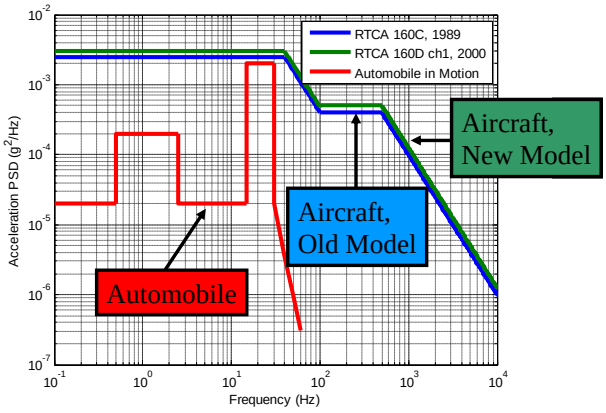

Figure 5: Vibration PSDs

V-5. PHASE JITTER FROM PHASE SCINTILLATION ($\sigma_{\delta\varphi p}$)

Similarly, the phase jitter induced by ionospheric phase scintillation can be found by substitute Eq. (1) into the second integrand of Eq. (5) as follows

$$\sigma^2_{\delta\varphi p} = \int_0^\infty |1 - H(j2\pi f)|^2 S_{\delta\phi_p}(f) df \quad radians^2. \tag{19}$$

A result of Eq. (19) in a closed form can be found in [1, 3, 28] with constraints imposed on the slope index p depending on the order of the closed loop PLL. In this work, p is chosen to be 2.5, which is a valid value based on the current data analysis [1]. If the constraints of p were not met based on the observations on the new data, one can numerically integrate Eq. (19) to obtain an approximate result.

V-6. DYNAMIC STRESS IN THE PLL (θ_e)

Because of an abrupt motion, the PLL would experience excessive phase error. Of interest is the peak error, i.e., the phase error transient response of the phase acceleration or phase jerk. For the second-order loop, the phase error due to dynamic stress (phase acceleration) is bounded by [page 180, 27]

$$\theta_{e2} = \frac{\dot{\Delta f}}{\omega_n^2} \quad cycles, \tag{20}$$

where $\dot{\Delta f}$ is a frequency ramp input in Hz/sec, and ω_n is the natural frequency of the closed loop in rad/sec. Convert the frequency ramp input into the phase acceleration in the line-of-sight direction, we have [16]

$$\theta_{e2} = 2\pi \frac{\dot{\Delta f}}{\omega_n^2} \cong 2\pi \frac{2.7599 a_{\max}}{\lambda_{carrier} B_n^2} \quad radians, \tag{21}$$

where $a_{\max}$ is the maximum value of line-of-sight phase acceleration in g, $\lambda_{carrier}$ is the wavelength of the carrier in meter.

Similarly, for the third-order loop the phase error from dynamic stress (phase jerk) is given by [page 390, 26]

$$\theta_{e3} = 2\pi \frac{\ddot{\Delta f}}{\omega_n^3} \cong 2\pi \frac{5.67 j_{\max}}{\lambda_{carrier} B_n^3} \quad radians, \tag{22}$$

where $j_{\max}$ is the maximum value of line-of-sight jerk experienced by the receiver in g/sec. In [24], $a_{\max}$ and $j_{\max}$ have been defined to regulate the performance of the GPS receivers used in aviations. Table 4 gives the values of $a_{\max}$ and $j_{\max}$ for aircrafts and automobiles (for comparison).

Table 4: Accelerations and Jerks

Aircraft (RTCA 229C)		Automobile (fast turns)	
amax (g)	jmax (g/sec)	amax (g)	jmax (g/sec)
0.5	0.25	0.3	0.38

V-7. RESIDUAL DYNAMIC STRESS FROM THE INERTIAL MEASUREMENTS (θ_{eaid})

If the PLL is inertial aided, the platform dynamics would be tracked by the inertial measurement unit (IMU). There is no need for the PLL to track high platform dynamics. As a result, the bandwidth of the PLL can be reduced such that more noise can be tolerated. However, the Doppler estimate provided by the IMU is not perfect. There is a residual Doppler estimate error leaking into the PLL. Therefore, this residual Doppler estimate error has to be tracked by the PLL. The amount of this Doppler estimate error depends on the quality of the IMU used for the carrier tracking loop aiding. This Doppler estimate can be modeled as either a frequency step error [12] or a frequency ramp error. In this work, we modeled the estimate error as a frequency ramp. The upper bound of the 3-sigma Doppler estimate error, $\Delta\dot{f}_{aid}$, can be found in [13]. The 3-sigma $\Delta\dot{f}_{aid}$ is 0.015 Hz/sec for a navigation grade IMU and 1.8 Hz/sec for an automotive grade IMU. The effect of this frequency ramp error is evaluated by examining the peak phase error of the tracking loop. Again, this transient peak error of both a second order and a third order PLLs given a frequency ramp input is bounded by the same form in Eq. (20) [page 390, 26 and page 180, 27]. Therefore,

$$\theta_{eaid} = 2\pi \frac{\Delta\dot{f}_{aid}}{\omega_n^2} = 2\pi \frac{\Delta\dot{f}_{aid}}{(1.885B_n)^2} \quad radians. \tag{23}$$

V-8. PHASE JITTER FROM THE G-SENSITIVITY OF THE LOCAL OSCILLATOR (θ_{acc})

In the case of aided tracking loops, the oscillator g-sensitivity must be considered. The frequency error, at the input of the tracking loop, induced by the g-sensitivity of the oscillator is expressed as [page 190, 27]

$$\Delta f_g = k_g f_{carrier} A(t) \quad Hz, \tag{24}$$

where k_g is the oscillator's g-sensitivity in parts/g (values given in Table 1), $f_{carrier}$ is the carrier frequency, and $A(t)$ is the acceleration stress in g as a function of time. If $A(t)$ is a jerk stress, g/sec, then the units of Δf_g are Hz/sec. As a result, Δf_g is a frequency ramp error goes into the PLL. Similar to the analysis for the error on the external Doppler estimate, we have the peak phase error of the tracking loop as

$$\theta_{acc} = 2\pi \frac{\Delta f_g}{\omega_n^2} = 2\pi \frac{\Delta f_g}{(1.885B_n)^2} \quad radians. \tag{25}$$

Until this step, we have analyzed of phase jitter for both unaided and aided PLL. Thus, we have each term of Eq. (4) for both cases. In the next section, the same analysis would be applied for the FLL.

VI. FREQUENCY-LOCKED LOOP (FLL) LINEAR MODEL ANALYSIS

A FLL used to be called an automatic frequency control (AFC) loop. The fundamental idea of a frequency discriminator is to measure the change in carrier phase over a finite interval of time. Various types of frequency discriminators have been investigated in [19]. Since the frequency discriminators are affected by the navigation databit, the sign changes between successive samples must be resolved. Among those AFC's, the cross-product AFC with decision feedback (CPAFCDF) would solve the bit changing problem as well as give the best noise performance [20]. As will be seen, the frequency estimate is achieved by performing cross-product on the successive in-phase (I) and quadrature (Q) samples. On the other hand, the sign change, used as a decision feedback to the tracking loop, is sensed by doing the dot-product of the successive I and Q samples. These sign changes can be used to demodulate the data differentially (differential phase shift keying (DPSK) demodulation) [page 381, 26]. In this work, we decoupled the analysis of the cross-product and the dot-product operations of the frequency tracking loop. The dot-product operation used as a DPSK demodulation will be discussed in Section VIIII. In this section, we focus on the frequency tracking loop without decision feedback. Since the FLL is used as a backup tracking loop for the application in this work, the bit synchronization has been done by the PLL before the receiver switches to the FLL. Accordingly, a cross-product AFC (CPAFC) would be the applicable to provide the frequency estimate. Figure 6 shows the block

diagram of the CPAFC [19]. As shown in [19], the frequency discriminator output is represented by

$$V_f(k) = I_{k-1}Q_k - Q_{k-1}I_k\,, \tag{26}$$

where I_k and Q_k are the baseband in-phase and quadrature samples at the outputs of the integrate-and-dump filters. The cross-product has to be performed within a databit period [page 379, 26]. Therefore, the maximum coherent integration time for this frequency tracking loop is half of the databit period. For example, T_{coh} is 10 msec for GPS tracking and 1 msec for WAAS tracking.

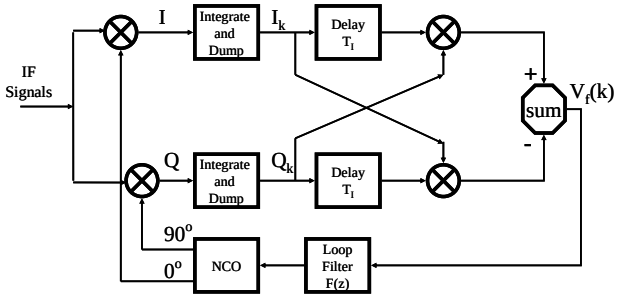

Figure 6: Cross Product AFC (CPAFC)

The linear mode of this type of FLL has exactly the same form as the PLL shown in Figure 4 except that the input is replaced by f_i , the output is f_o , and the frequency error estimate is defined as δf . It is important to note that the carrier NCO in a FLL does not act as an integrator. It is simply a means of converting a frequency number to sine and cosine of frequency [page 384, 26]. Therefore, the order of the closed loop is the same as the order of the loop filter. Traditionally, a second order FLL is used for a receiver, which can track a constant phase acceleration. From now on, we would like to focus on the error performance evaluation of this second order cross-product automatic frequency control loop.

Similar to the PLL, the 1-sigma frequency error is defined as frequency jitter [27], which is represented by

$$\sigma_{\delta f} = \sqrt{\sigma_{\delta f\omega}^2 + \sigma_{\delta fsv}^2 + \sigma_{\delta frx}^2 + \sigma_{\delta fv}^2 + \sigma_{\delta fp}^2} + \frac{\nu_e + \nu_{acc}}{3} \quad \text{Hz} \tag{27}$$

where

$\sigma_{\delta f\omega}$ = frequency jitter from thermal noise and amplitude scintillation (if applied);

$\sigma_{\delta fsv}$ = frequency jitter from the instability of the satellite's oscillators;

$\sigma_{\delta frx}$ = frequency jitter from the instability of the receiver's oscillators;

$\sigma_{\delta fv}$ = vibration induced frequency jitter;

$\sigma_{\delta fp}$ = frequency jitter caused by phase scintillation;

ν_e = dynamic stress in the FLL tracking loop

ν_{acc} = the excessive bias frequency error induced by the acceleration sensitivity of the local oscillator.

Each term of the error sources will be evaluated separately in the following sub-sections.

VI-1. THERMAL NOISE AND AMPLITUDE SCINTILLATION ($\sigma_{\delta f\omega}$)

Thermal noise tracking error of the FLL with a cross-product frequency discriminator is given by [page 381, 26] the following form,

$$\sigma_{\delta f\omega}^2 = \frac{1}{4\pi^2}\frac{4B_n}{T_{coh}^2\dfrac{C}{N_0}}\left[1+\frac{1}{2T_{coh}\dfrac{C}{N_0}}\right] \quad Hz^2\,. \tag{28}$$

Analog to the derivations in [page 92, 1 and 16], in the presence of amplitude scintillation, the tracking error was derived and given as follows

$$\sigma_{\delta f\omega}^2 = \frac{1}{4\pi^2}\frac{4B_n}{T_{coh}^2\dfrac{C}{N_0}(1-S_4^2)}\left[1+\frac{1}{2T_{coh}\dfrac{C}{N_0}(1-2S_4^2)}\right]$$

Hz^2 . (29)

As will be seen in the following sub-sections, the analysis for the remaining error sources is simply conducted by the following equation

$$\sigma_{\delta fx}^2 = \int_0^\infty \left|1-H(j2\pi f)\right|^2 S_{\delta f_x}(f)\,df \qquad Hz^2\,, \tag{30}$$

where $S_{\delta f_x}$ is the corresponding frequency noise PSD of each error source. Usually, the frequency noise PSD can be approximated by the phase noise PSD with the following relation:

$$S_{\delta f_x} = f^2 S_{\delta\phi_x}\,. \tag{31}$$

With Eqs. (30) and (31), and given the phase noise PSDs, the error performance of a second order FLL was analyzed and provided as follows.

VI-2. FREQUENCY JITTER FROM RECEIVER OSCILLATOR PHASE NOISE ($\sigma_{\delta frx}$)

$\sigma_{\delta frx}$ is calculated by substituting Eq. (12) into Eqs. (30) and (31). Since $S_{\delta f_x}$ is zero when $f \geq f_h$ and $f_h = \frac{1}{2T_{coh}}$, we can further simplify Eq. (30) as follows

$$\sigma^2_{\delta frx} = N^2\{Xh_4\int_0^{x_h}\frac{x^2}{1+x^4}dx + h_3\int_0^{x_h}\frac{x^3}{1+x^4}dx + \frac{h_2}{X}\int_0^{x_h}\frac{x^4}{1+x^4}dx + \frac{h_1}{X^2}\int_0^{x_h}\frac{x^5}{1+x^4}dx + \frac{h_0}{X^3}\int_0^{x_h}\frac{x^6}{1+x^4}dx\} \quad Hz^2, \tag{32}$$

where $X = \frac{2\pi}{\omega_n}$, $x_h = \frac{2\pi f_h}{\omega_n}$. Note that Eq. (32) is valid only for a second order FLL. Unlike the results in Eq. (15), Eq. (32) has to be calculated numerically.

VI-3. SATELLITE OSCILLATOR PHASE NOISE ($\sigma_{\delta fsv}$)

$\sigma_{\delta fsv}$ has the same form as in Eq. (32) except that the coefficients, h_i , are those values for the Cesium clock.

VI-4. VIBRATION INDUCED FREQUENCY JITTER ($\sigma_{\delta fv}$)

The frequency jitter induced by the platform vibration can be calculated by substituting Eqs. (18) and (31) into Eq. (30). The calculation was done also by a numerical method.

VI-5. FREQUENCY JITTER FROM PHASE SCINTILLATION ($\sigma_{\delta fp}$)

Similarly, the frequency jitter induced by ionospheric phase scintillation can be found by substituting Eqs. (1) and (31) into Eq. (30). Closed form solutions with constraints on the slope index p are available in [page 149, 1]. Alternatively, we can evaluate the result numerically if the constraints are not met.

VI-6. DYNAMIC STRESS IN THE FLL (ν_e)

Given the same order of the closed loop, the FLL can track one order higher of the dynamics than the PLL does [27]. Therefore, the peak frequency error of the second-order FLL due to a range (phase) jerk input can be bounded by the following form [page 192, 27]

$$\nu_e = \frac{\ddot{\Delta f}}{\omega_n^2} = \frac{2.7599\, j_{\max}}{\lambda_{carrier} B_n^2} \quad Hz, \tag{33}$$

where $j_{\max}$ is the maximum line-of-sight phase jerk in g/sec.

VI-7. RESIDUAL DYNAMIC STRESS FROM THE INERTIAL MEASUREMENTS (ν_{eaid})

We model the residual error of the external Doppler estimate to be a frequency ramp. Therefore, of interest is the peak frequency error caused by a frequency ramp input in the second-order FLL. For a FLL, the steady state error is given by the first derivative of the phase error in the second-order PLL. The response of the frequency step input to a second-order PLL is [page 192, 27]

$$\theta = 0.45\frac{\Delta f_{aid}}{\omega_n} \quad cycles, \tag{34}$$

where Δf_{aid} is the frequency step input. Performa one derivative on Eq. (34), we obtain the response of the second-order FLL due to a frequency ramp input. Thus,

$$\nu_{eaid} = 0.45\frac{\dot{\Delta f}_{aid}}{1.885 B_n} \quad Hz. \tag{35}$$

VI-8. FREQUENCY JITTER FROM THE G-SENSITIVITY OF THE LOCAL OSCILLATOR (ν_{acc})

The frequency error, at the input of the tracking loop, induced by the g-sensitivity of the oscillator has been given in Eq. (24). If the induced frequency error is a frequency ramp, the final frequency jitter has the same form of Eq. (35). Therefore,

$$\nu_{acc} = 0.45\frac{\Delta f_g}{1.885 B_n} \quad Hz, \tag{36}$$

where Δf_g here is the frequency ramp induced by the g-sensitivity of the local oscillator in the presence of a constant range (phase) jerk dynamics.

VII. RESULTS AND DISCUSSIONS OF THE LINEAR MODEL ANALYSIS

Thus far, we have completed the linear model analysis for both the PLL and the FLL. It is doable to find the minimum C/N_0 based on the first two requirements mentioned in Section I. The minimum allowable C/N_0 would be obtained by examining where the tracking threshold is exceeded. The rule-of-thumb threshold for a PLL is 15 degree and for a FLL is $\frac{1}{12T_{coh}}$ [27]. Figures 7 to 10 show the individual components of the phase jitter in Eq. (4) and the frequency jitter in Eq. (27). Note that the frequency jitter on Figures 9 and 10 has been normalized by multiplying Eq. (27) with the coherent integration time, T_{coh}. Therefore, it is dimensionless and the tracking threshold is 1/12. The red shaded area in each figure represents the allowable region given a C/N_0 without inertial aiding. Accordingly, the blue shaded area represents the allowable region given a C/N_0 when the tracking loop is inertially aided. Obviously, one wants a larger shaded region; as a result, the noise bandwidth can be reduced much lower such that there are more margins for interference. In short, Figures 7 to 10 emphasize the following three important facts.

1. Applying an inertial aiding on the carrier tracking loops does improve the tracking performance under a dynamical environment. This is shown by comparing the red shaded wage area to the blue shaded area in Figures 7 to 10.
2. However, the above improvement is restricted by the oscillator's g-sensitivity (can be seen from curves which lower-bound the blue shaded area in Figures 7 and 9). Using a low g-sensitivity oscillator for an inertial aided tracking loop does greatly enhance the benefits gained by the inertial aiding technique.
3. In terms of the probability losing lock, the improvement in the margin for a lower C/N_0 by the inertial aiding technique on a FLL is much larger than that of a PLL. This argument can be seen by comparing the blue shaded area of Figures 7 and 8 to Figures 9 and 10, respectively. However, one should be aware that the absolute measurements made by the FLL are nosier than those from the PLL.

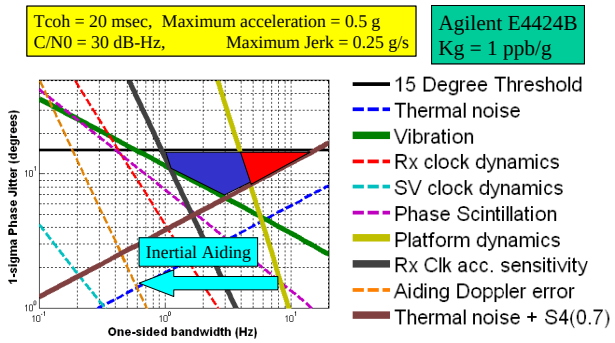

Figure 7: 3rd Order PLL, individual phase error component, normal g-sensitivity oscillator

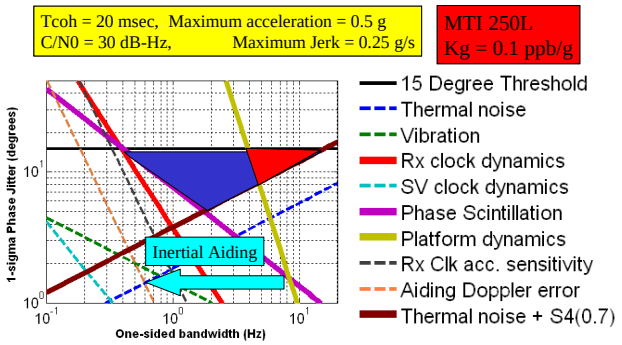

Figure 8: 3rd Order PLL, individual phase error component, low g-sensitivity oscillator

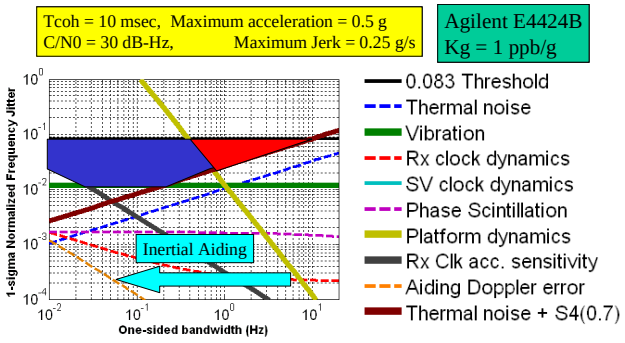

Figure 9: 2nd Order FLL, individual normalized frequency error component, normal g-sensitivity oscillator

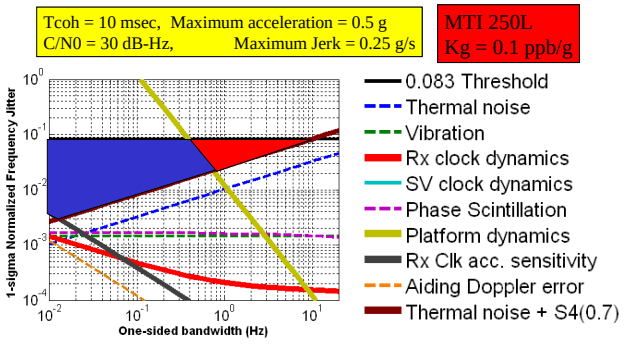

Figure 10: 2nd Order FLL, individual normalized frequency error component, low g-sensitivity oscillator

With a fixed C/N_0, one can find two allowable noise bandwidths (a pair of higher-bound and lower-bound bandwidths) such that the jitter is blow the tracking threshold. For example, in Figure 7, the higher-bound bandwidth is near 15 Hz, any bandwidth above this higher-bound bandwidth, the phase jitter would be larger than the threshold and the phase jitter is mainly contributed by thermal noise and amplitude scintillation effects. On ther other hand, the lower-bound bandwidth in Figure 7 is close to 7 Hz. The phase jitter would be dramatically increased, contributed by all of the remaining error sources, if the bandwidth is below the lower-bound bandwidth. If searching over the combinations of the noise bandwidth and C/N_0, one would obtain a "feasible B_n *vs* C/N_0 contour" shown in Figure 11. The boundary of the contour shows the combination of B_n *and* C/N_0 where the jitter is at the tracking threshold. Any combinations inside the feasible region guarantee that the tracking performance is acceptable. By this contour, it is easy to find the minimum allowable C/N_0 and its corresponding noise bandwidth. Figure 12 shows the contours for both the PLL and FLL processing WAAS signals with and without inertial aiding. Figure 12 also emphasizes that the improvement obtained by inertial aiding for the FLL is superior to the PLL. The quantitative results will be given at the end of this paper in tables.

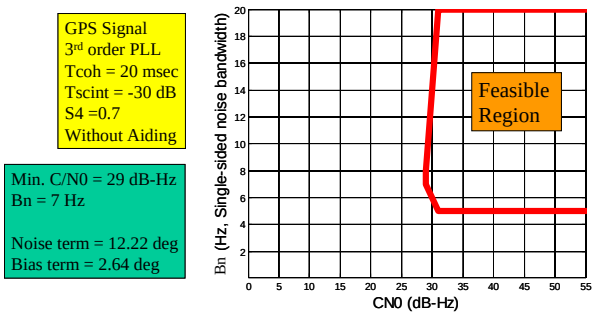

Figure 11: Feasible Bn vs C/N0 Contour

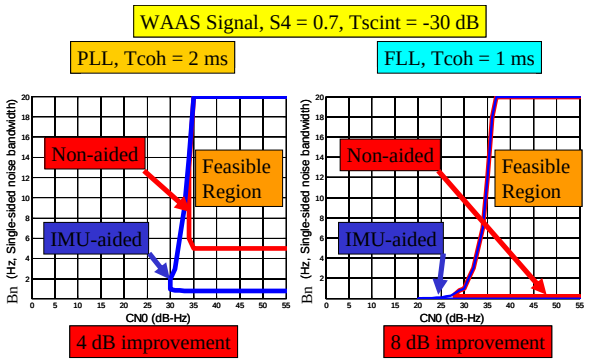

Figure 12: Feasible Bn vs C/N0 Contour, showing C/N0 improvements obtained by the inertial aiding

Given the conditions which achieve the minimum C/N0, we want to know if the WER requirement is satisfied or not. If the WER were not met, we would like to find at which C/N0 the WER requirement will be met. In the second half of this paper, work has been done to estimate a justifiable WER for both GPS and WAAS signals using either the PLL or the FLL tracking loops.

VIII. BIASED PROBABILITY DENSITY FUNCTION (PDF) OF A PLL

To evaluate the average bit error rate (BER) conditioned on the phase estimate error, it is required to solve the PDF of the phase estimate error in a PLL. The steady state PDF of the first-order PLL has been found by solving its corresponding Fokker-Planck equation [page 89, 37]. The PDF of the first-order PLL is also called Tikhonov density function. However, the Tikhonov density function was obtained by assuming no dynamic stress imposed on the first-order PLL. We are interested to find the PDF when the tracking loop is dynamically stressed. Using the stressed PDF would more accurately predict the BER for this aviation application of a GPS/WAAS receiver.

The steady state PDF of the **standard** first-order PLL is given as follows [page 89, 37]

$$p_\phi(\phi) = C\exp(\alpha\cos(\phi)+\beta\phi)[1+ D\int_{-\pi}^{\phi}\exp(-\alpha\cos(x)-\beta x)dx] \quad -\pi \le \phi \le \pi \tag{37}$$

with the boundary condition

$$p_\phi(\pi) = p_\phi(-\pi), \tag{38}$$

and the normalizing condition

$$\int_{-\pi}^{\pi} p_\phi(\phi)d\phi = 1. \tag{39}$$

ϕ is the phase estimate error, which is $\delta\varphi$ in the previous sections. C and D are constants which can be resolved by the given boundary and normalizing conditions. α and β are related to the variance and the dynamic stress of the phase jitter by the following forms.

$\alpha = \frac{1}{\sigma_\phi^2}$ and $\beta = \frac{\theta_e}{\sigma_\phi^2}$, where σ_ϕ^2 is the variance of the noise component in the phase jitter in Eq. (4), and θ_e is the constant dynamics stress in the bias component of the

phase jitter. If there is no dynamic stress, $\beta = 0$, Eq. (37) becomes the well known Tikhonov density function [page 90, 37] written as

$$p_\phi(\phi) = \frac{\exp(\alpha\cos(\phi))}{2\pi I_0(\alpha)} \qquad -\pi \le \phi \le \pi\,, \tag{40}$$

where $I_0(\bullet)$ is the zeroth-order modified Bessel function. For the **Costas** PLL, the phase estimate error ϕ and θ have to double to account for the dot-product of the in-phase and quadrature channels. Accordingly, the PDF of the first-order Costas PLL is given as [page 274, 38]

$$p_\phi(\phi) = \frac{\exp(\alpha_c\cos(2\phi))}{\pi I_0(\alpha_c)} \qquad -\frac{\pi}{2} \le \phi \le \frac{\pi}{2}\,, \tag{41}$$

where $\alpha_c = \dfrac{1}{4\sigma_\phi^2}$.

If there is a dynamic stress, for the Costas loop, $\beta = \beta_c = \dfrac{\theta_e}{2\sigma_\phi^2}$. Similar to Eq. (37), we can find the expression for the stressed PDF of the **Costas** loop as

$$p_\phi(\phi) = C_c \exp(\alpha_c\cos(2\phi) + 2\beta_c\phi)[1 + D_c \int_{-\pi/2}^{\phi} \exp(-\alpha_c\cos(2x) - 2\beta_c x)dx] \qquad -\frac{\pi}{2} \le \phi \le \frac{\pi}{2}\,. \tag{42}$$

From the boundary condition, $p_\phi(\frac{\pi}{2}) = p_\phi(-\frac{\pi}{2})$, the constant D_c can be found as

$$D_c = \frac{\exp(-2\beta_c\pi) - 1}{\int_{-\pi/2}^{\pi/2} \exp(-\alpha_c\cos(2x) - 2\beta_c x)dx}\,. \tag{43}$$

Given D_c and from the normalizing condition, $\int_{-\pi/2}^{\pi/2} p_\phi(\phi)d\phi = 1$, the constant C_c can be found as

$$C_c = \frac{1}{\int_{-\pi/2}^{\pi/2} E(\phi)[1 + D_c F(\phi)]d\phi}\,, \tag{44}$$

where

$$E(\phi) = \exp(\alpha_c\cos(2\phi) + 2\beta_c\phi)$$

$$F(\phi) = \int_{-\pi/2}^{\phi} \exp(-\alpha_c\cos(2x) - 2\beta_c x)dx\,.$$

A numerical computation is required to evaluate Eq. (42). In the case of the Costas PLL, it is important to note that for $\dfrac{\beta_c}{\alpha_c} = \theta_e > \sin(\dfrac{\pi}{4})$, the steady state solution does not hold and for $\alpha_c > 1$, the PDF gives more reasonable accuracy [page 93, 37]. One can find that if $\theta_e = 0$, i.e., no dynamic stress, Eq. (42) would become Eq. (41). Also note that the closed form of a stressed PDF given in [page 118, 38] is incorrect. One can simply confirm this by doing the normalizing condition test. Figure 13 shows the main idea of this section. Both curves are the PDF with the same amount of phase jitter. The blue curve stands for the non-stressed PDF while the red curve represents the stressed PDF. Obviously from Figure 13, the BER is different for each case. It would be too optimistic if one ignores the bias phase error due to dynamics. On the other hand, it is pessimistic if one treats the bias term as a part of the total noise component. In the later case, one would obtain exactly the same BER because the BER is evaluated at the same value of the total phase jitter no matter the tracking loop is dynamically stressed or not. Accordingly, it would mislead one to the following wrong statement saying that applying an inertial aiding to the carrier tracking loop would not improve the BER at all since the blue curve is always the case.

The above arguments apply to the PDF of the FLL too. Unfortunately, the PDF of a FLL has not been solved. Solving for the PDF and the statistic of losing lock of the FLL is an important future work after this study.

Thus far, we can calculate the BER conditioned on the phase estimate error for the PLL tracking loop. In contrast, for the FLL tracking loop, we will use the traditional DPSK upper bound BER, which assumes zero frequency estimate error. In the Section VIIII, details about the BER and WER will be discussed.

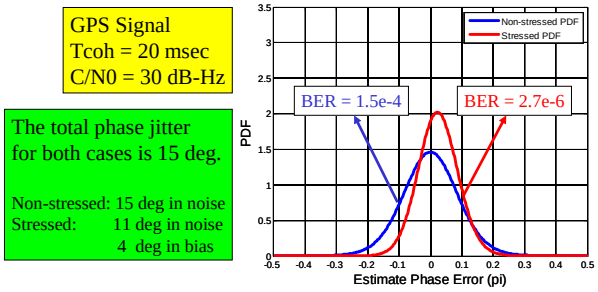

Figure 13: The PDF of a dynamically stressed PLL

VIIII. BIT ERROR RATE (BER), WORD ERROR RAATE (WER), AND BURST ERROR PROPERTY OF WAAS WER

In this section, we would like to evaluate BER and WER for both GPS and WAAS data with both PLL and FLL tracking loops.

VIIII-1. BER

The evaluation of the BER for both GPS and WAAS will be divided in two folds here. The first one is the BPSK demodulation BER for the PLL tracking and the second one is the DPSK demodulation for the FLL tracking.

VIIII-1-1. BER in the case of a PLL tracking without scintillation

As the same in Section VIII, define ϕ the phase estimate error. The BER for the GPS messages using a PLL tracking is given by the expression for BPSK [38]

$$P_{b,GPS,PLL}(\phi) = \frac{1}{2} erfc(\sqrt{T_{GPS,PLL}\frac{C}{N_0}}\cos(\phi)), \qquad (45)$$

where $T_{GPS,PLL}$ is the coherent integration time and it has to be the bit period of the GPS databit, which is 0.02 sec, and the complementary error function, $erfc(\bullet)$, is defined as

$$erfc(x) = \frac{2}{\sqrt{\pi}}\int_x^\infty e^{-y^2} dy . \qquad (46)$$

It is also BPSK for WAAS signal except that there is an convolutional encoding with rate 1/2 and constraint length 7 imposed on WAAS messages. Therefore, there are 500 symbols/sec used to represent the 250 bits/sec WAAS databits. Applying the convolutional encoding can somewhat compensate the loss in bit energy due to its faster data rate. The BER of WAAS messages using the PLL tracking can be upper-bounded by [page 199, 39]

$$P_{b,WAAS}(\phi) \le \frac{1}{2}[36D^{10} + 211D^{12} + 1404D^{14} + 11633D^{16}], \qquad (47)$$

where for the coherent BPSK signal with soft decision for the Viterbi decoding [page 196, 39],

$D = \exp(-T_{WAAS,PLL}\frac{C}{N_0}\cos^2(\phi))$, and $T_{WAAS,PLL}$ is the symbol period of the WAAS message, 0.002 sec.

Therefore, the average bit error probability (BER) for GPS and WAAS is given by averaging $P_b(\phi)$ over the phase error distribution given in Eqs. (41) and (42) for no dynamic stress and with dynamic stress, respectively.

$$BER_{PLL} = \int_{-\pi/2}^{\pi/2} P_b(\phi) p_\phi(\phi) d\phi . \qquad (48)$$

VIIII-1-2. BER in the case of a PLL tracking with scintillation

In the presence of scintillation, the signal amplitude has the Nakagami-m distribution given in Eq. (3). The BER in this case is [page 204, 1]

$$BER_{PLL,sc\,int} = \int_0^\infty \int_{-\pi/2}^{\pi/2} P_b(\phi, A) p_\phi(\phi) f_A(A) d\phi dA . \qquad (49)$$

Further simplifications on Eq. (49) can be found in [page 204, 1]. The final BER with PLL tracking in the presence of scintillation is

$$BER_{PLL,sc\,int} = \int_0^\infty \int_{-\pi/2}^{\pi/2} P_b(\phi, \rho_0) p_\phi(\phi) f_{\rho_0}(\rho_0) d\phi d\rho_0 , \qquad (50)$$

where

$$f_{\rho_0}(\rho_0) = \frac{m^m \rho_0^{m-1}}{\Gamma(m)\left(\frac{C}{N_0}\right)^m}\exp\left(-\frac{m\rho_0}{\frac{C}{N_0}}\right)$$ and ρ_0 represents

the instantaneous carrier to noise density ratio of the received signal;

$P_\phi(\phi)$ is the PDF defined in Eq. (41) and (42);

for GPS ($T_{GPS,PLL}$ = 0.02 sec):

$P_b(\phi,\rho_0)=\frac{1}{2}erfc(\sqrt{T_{GPS,PLL}\rho_0}\cos(\phi))$, and

for WAAS ($T_{WAAS,PLL}$ = 0.002 sec):

$P_b(\phi,\rho_0)=$ the right hand side of Eq. (47) with

$D=\exp(-T_{WAA\$PLL}\rho_0\cos^2(\phi))$.

VIIII-1-3. BER in the case of a FLL tracking without scintillation

The navigation databit demodulation is achieved by sensing the successive sign changes, the dot-product operation, of the in-phase channel [page 381, 26]. Therefore, it is a DPSK demodulation. The maximum coherent integration time of the FLL is limited to be half of the symbol period. As defined, δf is the frequency estimate error of the FLL. Thus, the phase error after a period of the coherent integration time of the FLL is $2\pi\delta f T_{FLL}$ in radians. Given this amount of phase error, the conditional probability of bit error is given as [40 and Eq. (5.4-54) of 41]

$$P_{b,FLL}(\delta f)=Q_1(a,b)-\frac{1}{2}e^{-(a^2+b^2)/2}I_0(ab),$$

$$a=\sqrt{T_{FLL}\frac{C}{N_0}(1-\cos(2\pi\delta f T_{FLL}))},$$
$$b=\sqrt{T_{FLL}\frac{C}{N_0}(1+\cos(2\pi\delta f T_{FLL}))}, \quad (51)$$

where $Q_1(\bullet)$ is the well-known first-order Marcum's Q function, $I_0(\bullet)$ is the zeroth-order modified Bessel function, and T_{FLL} = 0.01 sec for GPS signal.

If we assume zero frequency estimate error, $\delta f=0$, Eq. (51) reduces to the traditional probability of bit error of a DPSK signal as [page 381, 26]

$$P_{b,FLL}=\frac{1}{2}e^{-T_{FLL}\frac{C}{N_0}}. \quad (52)$$

Since the distribution of δf is not available, Eq. (51) will only be useful once the PDF of the FLL is obtained. Hence, Eq. (52) would be the BER of a GPS signal with the FLL tracking.

The BER of a WAAS message with a FLL tracking also follows the upper bound given in Eq. (47) except that the coefficient, D, is not as given as mentioned above. A soft decision is not applicable in this case since the DPSK demodulation only gives the sign changes between the successive databits. Accordingly, a hard decision is used and this results in the Binary Symmetric Channel (BSC) [page 196, 39]. For a BSC channel, the coefficient D was found by applying the maximum-likelihood metric. The result of this D is called the union-Bhattacharyya error bound and given as [page 198, 39 and page 107, 42]

$$D=\sqrt{4P_{b,FLL}(1-P_{b,FLL})}. \quad (53)$$

Note that T_{FLL} =0.001 sec for WAAS signal with a FLL tracking here.

In short, the BER of GPS message with a FLL tracking is predicted by Eq. (52). The BER of WAAS message with a FLL tracking is given by substituting Eqs. (53) and (52) into Eq. (47).

VIIII-1-4. BER in the case of a FLL tracking with scintillation

Similarly, in the presence of scintillation, the signal amplitude has the Nakagami-m distribution given in Eq. (3). However, the BER for the FLL tracking is not averaged over the distribution of the frequency estimate error. Thus, Eq. (52) will used to determine the BER in this case. The BER is, therefore,

$$BER_{FLL,scint}=\int_0^\infty P_{b,FLL}(\rho_0)f_{\rho_0}(\rho_0)d\rho_0, \quad (54)$$

where

$$f_{\rho_0}(\rho_0)=\frac{m^m\rho_0^{m-1}}{\Gamma(m)\left(\frac{C}{N_0}\right)^m}\exp\left(-\frac{m\rho_0}{\frac{C}{N_0}}\right)$$ and ρ_0 represents the instantaneous carrier to noise density ratio of the received signal;

for GPS (T_{FLL} = 0.01 sec):

$P_{b,FLL}(\rho_0)=\frac{1}{2}e^{-T_{FLL}\rho_0}$, and

for WAAS (T_{FLL} = 0.001 sec):

$P_{b,FLL}(\rho_0)=$ the right hand side of Eq. (47) with

$$D = \sqrt{4 \cdot \frac{1}{2} e^{-T_{FLL}\rho_0} (1 - \frac{1}{2} e^{-T_{FLL}\rho_0})} .$$

Finally, we have completed the evaluation the BER for both GPS and WAAS using either a PLL or a FLL tracking in the environment with or without ionospheric scintillation. Of interest are the word error rates for GPS and WAAS messages.

VIII-2. WER AND BURST ERROR PROPERTY OF WAAS WER

VIII-2-1. WER FOR GPS

The word error rate for GPS data may be approximated using

$$WER = 1 - (1 - BER)^M , \quad (55)$$

where $M = 30$ for a GPS word. The assumption for Eq. (55) is that the probability of bit error in successive bits is independent. Without scintillation, this assumption is reasonable. However, in the presence of scintillation, the independency holds only for a fast scintillation [page 209, 1]. For example, if the fading stands for 0.6 sec, the signal amplitude for the whole GPS follows the Nakagami-m distribution. In this case, the WER predicted by Eq. (55) would be too conservative. In this paper, a very deep fading scenario was considered and the fading period is much less than 0.6 sec. Hence, Eq. (55) was used to approximate the WER. The details of the case of slow scintillation can be found in [page 209, 1].

VIII-2-2. WER FOR WAAS

The WER of WAAS messages will likely to happen in bursts because of the Viterbi decoding of the convolutional code. Eq. (55) would give a conservative result even in the case of fast scintillation. The burst property of Viterbi decoding has been studied in [43, 44, 45, and 46]. Specifically, in [43 and 44], an algorithm was proposed to estimate the WER given the BER at the output of the Viterbi decoder. In the follows, we would do a quick summary of the algorithm without details.

Before listing the steps of the algorithm, it is important to define an error burst. CCITT [47] defines an error burst as "*a group of bits in which two successive erroneous bits are always separated by less than a given number (L) of correct bits.*" The number L is also called "Burst Length Criterion" (BLC) [43]. Here are the steps of the algorithm given in [43].

1. Calculate the BER at the output of the Viterbi decoder, i.e., those BER's for WAAS messages in the previous paragraphs
2. Let BLC = K-1, where K is the constraint length of the convolutional encoding. For WAAS messages, K=7.
3. Define an important measure of a code's burst error performance, called "Average Burst Length, $\overline{B}$ ".

   $$\overline{B} = \frac{Total \quad length \quad of \quad all \quad bursts}{Total \quad number \quad of \quad bursts}$$

   From simulation results for BLC=6 and the asymptotic limit, $\overline{B}$ is approximated by

   $$\overline{B} = 5 + \frac{17.1}{\left(\sqrt{-\log_{10}(2BER)} + 0.0475 \log_{10}(2BER) + 0.3161 (\log_{10}(2BER))^2 \right)} \quad (56)$$

4. Burst Length Distribution: Based on computer simulations with comparatively low E_b/N_0, the PDF of error burst lengths is

   $$p(l) = \frac{1}{\overline{B}} \left(1 - \frac{1}{\overline{B}} \right)^{l-1} . \quad (57)$$

5. Density of Errors in a Burst: The average density of errors in a burst of length l is given as

   $$\vartheta(l) = \begin{cases} 1 , & l = 1 \\ \dfrac{l+2}{2l} , & l > 1 \end{cases} . \quad (58)$$

6. Average Density for all Burst: The average density of errors in all bursts can be defined as

   $$\overline{\vartheta} = \frac{Total \quad number \quad of \quad errors}{Total \quad length \quad of \quad all \quad bursts}$$

   This is further expressed as

   $$\overline{\vartheta} = \frac{\sum_l \left(l \cdot p(l) \cdot \vartheta(l) \right)}{\sum_l \left(l \cdot p(l) \right)} . \quad (59)$$

7. The final WER (burst error probability) is then defined as

$$WER = \frac{BER}{B\vartheta} \qquad (60)$$

X. RESULTS AND DISSCUSIONS

With the above model analysis, we finally determined the minimum C/N_0 which would satisfy the three requirements, the PLL and FLL linear tracking thresholds as well as the required WER, which is less than 10^-4. Table 5 and Table 6 show the result for GPS and WAAS, respectively. The numbers in red represent the required C/N_0 for satisfying the linear threshold while those in green represent the required C/N_0 to meet the WER requirement.

It is important to emphasize that the results shown here are based on the low g-sensitivity oscillator, which gives 4 dB improvement comparing to the case of using normal g-sensitivity oscillators when the tracking loop is inertially aided.

The follows are the important information depicted by Table 5 and Table 6.

1. Based on the criteria of linear tracking thresholds, the technique of inertial aiding on the tracking loops provides 7 dB improvement for the PLL while there is 12 dB improvement for the FLL when there is no scintillation.
2. In the presence of scintillation, there is only 3 to 4 dB improvement by the inertial aiding on the PLL. However, there is still 8 to 9 dB improvement by the inertial aiding on the FLL.
3. The same trend in 1. and 2. applies to both GPS and WAAS.
4. Considering the WER requirement, the allowable C/N_0 based on tracking threshold does not give the required WER for all cases.
5. Furthermore, in the presence of scintillation, satisfying the WER requirement demands a much higher C/N_0, especially for WAAS. In this case it is reasonable to assume a zero phase or frequency estimate. Otherwise, a higher value of C/N_0 would be obtained.
6. However, it is unlikely that the downlinks from well separated geostationary satellites broadcasting WAAS will be affected simultaneously by local ionospheric scintillation. The loss of the WER requirement in one downlink may not be a severe threat to WAAS applications.
7. These high C/N_0 values resulted from evaluating the BER over the Nakagami-m distribution of the amplitude scintillation. It suggests that the distribution used for amplitude scintillation is too conservative.
8. The upper bound of the bit error rate for WAAS given in Eq. (47) is accurate only for high C/N_0. One can find that the result of Eq. (47) for WAAS using a PLL would be larger than 0.5 if C/N_0 is below 25 dB-Hz even assuming zero phase error. Therefore, one would not see any model results promising the WER requirement given a C/N_0, which is below 25 dB-Hz (for WAAS).

Table 5: Minimum required C/N0 for GPS

Min C/N0 satisfying both linear tracking threshold and WER
Rx: OCXO (MTI 250L), Navigation grade IMU

GPS Min. C/N0/ WER	PLL		FLL	
	Non-aided	IMU-aided	Non-aided	IMU-aided
No Scintillation	23	16	17	5
	28	28	31	31
S4=0.7 Tscint= -30 dB	29	26	26	15
	44*	44*	49*	49*

* Evaluated by assuming zero phase or frequency error

Table 6: Minimum required C/N0 for WAAS

Min C/N0 satisfying both linear tracking threshold and WER
Rx: OCXO (MTI 250L), Navigation grade IMU

WAAS Min. C/N0/ WER	PLL		FLL	
	Non-aided	IMU-aided	Non-aided	IMU-aided
No Scintillation	25	20	18	10
	28	28	29	29
S4=0.7 Tscint= -30 dB	34	30	28	20
	53*	53*	63*	63*

* Evaluated by assuming zero phase or frequency error

XI. CONCLUSIONS AND FUTURE WORK

On the whole, based on the criteria of the linear tracking thresholds, the minimum allowable C/N_0 for WAAS using an inertially aided FLL is 10 dB lower than using an inertially aided PLL. It suggests that using an inertially aided FLL is effective to cope with a fast and deep scintillation channel. However, the WER requirement indeed limits what has been gained by using an inertially aided FLL instead of using an inertially aided PLL.

The future work would be to investigate a tighter bound on predicting the BER or to run Monte Carlo simulations. The effects of using the FLL as a backup tracking on the code carrier smoothing are also important. It is crucial to know if this switching carrier tracking loops can still provide acceptable smoothing gain on the code measurement. We also suggest that re-examining the distribution of amplitude scintillation is needed. Last, solving for the PDF of the FLL is of interest too.

In conclusion, using an inertially aided FLL as a backup carrier tracking is an effective method to cope with ionospheric scintillation problems.

XII. ACKNOWLEDGMENTS

The authors gratefully acknowledge the sponsor of this research at Stanford University, the FAA satellite navigation product team.

We are sincerely grateful to Dr. Francis Natali for his advice on this paper and especially for his comprehensive comments on the analysis of the frequency-locked loop. Special thanks go to Dr. Jason Rife at Stanford University for his knowledgeable commentary on the statistical analysis of this paper. For Alireza Razavi (University of Minnesota, Twin Cities), much appreciation is due to for his constructive comments and advice.

XIII. REFERENCES

1. Knight, M.F., Ionospheric Scintillation Effects on Global Positioning System Receivers, *Ph.D. Thesis, The University of Adelaide, Adelaide, South Australia*, December, 2000.
2. Knight, M.F. and Finn, A., "The Effects of Ionospheric Scintillations on GPS," *Proc. ION GNSS 1998*, pp. 673-685.
3. Conker, R.S., El-Arini, M.B., and et al, "Modeling the Effects of Ionospheric Scintillations on GPS/SBAS Availability," *Proc. ION AM 2000*, pp. 563-576.
4. Humphreys, T.E., Psiaki, M. L., and et al, "GPS Carrier Tracking Loop Performance in the presence of Ionospheric Scintillations," *Proc. ION NTM 2005*, pp. 156-167.
5. Pullen, S., Opshauh, G., and et al, "A Preliminary Study of the Effect of Ionospheric Scintillation on WAAS User Availability in Equatorial Regions," *Proc. ION GNSS 1998*, pp. 687-699.
6. Yu, W., Lachapelle, G., and Skone, S., " PLL Performance for Signals in the Presence of Thermal noise, Phase noise, and Ionospheric Scintillation," Proc. ION GNSS 2006
7. Morrissey, T.N., Shallberg, K.W., and et al, "GPS Receiver Performance Characterization Under Simulated Ionospheric Scintillation Environments," *Proc. ION AM 2000*, pp. 577-587.
8. Morrissey, T.N., Shallberg, K.W., and et al, "GPS Receiver Performance Characterization Under Simulated Ionospheric Scintillation Environments II," *Proc. ION NTM 2002*, pp. 682-693.
9. Van Dierendonck, A.J., "Measuring Ionospheric Scintillation in the Equatorial Region Over Africa, Including Measurements From SBAS Geostationary Satellite Signals," *Proc. ION NTM 2004*, pp. 316-324.
10. So, H., Kee, C., and Kim, T., "Analysis of GPS Receiver Tracking Loss under Ionospheric Scintillation," *Seoul National University - Stanford University Student Joint Workshop*, June, 2006.
11. Hegarty, C.J., "Analytical Derivation of Maximum Tolerable In-Band Interference Levels for Aviation Applications of GNSS," *Journal of The Institute of Navigation, Vol. 44, No. 1*, pp. 25-34, Spring 1997.
12. Gebre-Egziabher, D., Razavi, A., and et al, "Sensitivity and Performance Analysis of Doppler-Aided GPS Carrier –Tracking Loops," *Journal of The Institute of Navigation, Vol. 52, No. 2*, pp. 49-60, Summer 2005.
13. Alban, S., Akos, D.M., and et al, "Performance Analysis and Architectures for INS-Aided GPS Tracking Loops," *Proc. ION NTM 2003*, pp. 611-622.
14. Alban, S., Design and Performance of a Robust GPS/INS Attitude System for Automobile Applications, *Ph.D. Thesis, Stanford University, Stanford, California, U.S.A.*, June, 2004.
15. Razavi, A., Sensitivity and Performance Analysis of Doppler-Aided GPS Carrier Tracking Loops, *M.S. Thesis, University of Minnesota, Twin Cities, Minneapolis, Minnesota*, October, 2005.
16. Chiou, T.Y., "GPS Receiver Performance Using Inertial-Aided Carrier Tracking Loop," *Proc. ION GNSS 2005*, pp. 2895-2910.
17. Irsigler, M. and Eissfeller, B., "PLL Tracking Performance in the Presence of Oscillator Phase Noise," *GPS Solutions, Volume 5, Number 4, Spring 2002*, Wiley Periodicals Inc., 2002
18. Cahn, C.R., "Improving Frequency Acquisition of a Costas Loop," *IEEE Transactions Communications, Vol. COM-25, No. 12*, pp. 1453-1459, December 1977.
19. Natali, F.D., "AFC Tracking Algorithms," *IEEE Transactions Communications, Vol. COM-32, No. 8*, pp. 935-947, August 1984.
20. Natali, F.D., "Noise Performance of a Cross-Product AFC with Decision Feedback for DPSK Signals," *IEEE Transactions Communications, Vol. COM-34, No. 3*, pp. 303-307, March 1986.
21. Ward, P.W., "Performance Comparisons Between FLL, PLL and a Novel FLL-Assisted-PLL Carrier

Tracking Loop Under RF Interference Conditions," *Proc. ION GNSS 1998*, pp. 783-795.
22. Van Dierendonck, A.J., "Technical Note on Assessment of CNAV Satellite Navigation using the C-Band," personal communication.
23. Razavi, A., Gebre-Egziabher, D., and Akos, D.M., "Tracking Weak GPS Signals: A methodology for Analysis and Experimental Validation," *IEEE Transactions on Aerospace and Electronic Systems, Vol. 43, No. 4*, 2007.
24. RTCA, Minimum Operational Performance Standards for Sensors Using GPS/WAAS, *RTCA Document No. RTCA/DO-229*, January 1996.
25. Misra, P., and Enge, P., Global Positioning System: Signals, Measurements, and Performance, Second Edition, *Ganga-Jamuna Press*, 2006
26. Van Dierendonck, A.J., "GPS Receivers," in *Global Positioning System: Theory and Applications, Vol. 1, AIAA, Washington, DC, 1996*, pp. 330-433.
27. Ward, P.W., "Satellite Signal Acquisition, Tracking, and Data Demodulation," in *Understanding GPS Principles and Applications, Second Edition, Artech House, Washington, DC, 2006*, pp. 153-241.
28. Rino, C.L., "A Power Law Phase Screen Model for Ionospheric Scintillation: 1. Weak Scatter," *Radio Science, Vol. 14, No. 6*, pp. 1135-1145, 1979a.
29. Fremouw, E.J., and et al, "On the Statistics of Scintillating Signals," *Journal of Atmospheric and Terrestrial Physics," Vol. 42*, pp. 717-731, 1980.
30. Conker, R.S., El-Arini, M.B., and et al, "Modeling the Effects of Ionospheric Scintillations on GPS/WAAS Availability," *MITRE Working Note Number WN00W22*, 2000.
31. Spilker, J., Digital Communication by Satellite, *Prentice-Hall, Cambridge, Massachusetts*, pp. 336-397, 1977
32. Gardner, F.M., Phaselock Techniques, *Third Edition, John Wiley & Sons*, pp. 143-182, 2005.
33. Grebenkemper, C.J., "Local Oscillator Phase Noise and its Effect on Receiver Performance," *Watkins-Johnson Company Tech-notes, vol. 8, No. 6*, Nov/Dec, 1981.
34. US Department of Defense, Global Positioning System Standard Positioning Service Signal Specification, Appendix A, Second Edition, June, 1995.
35. Hamkins, J., "A Joint Receiver-Decoder for Convolutionally Coded BPSK," *The Telecommunications and Mission Operations Progress Report, Vol. 42-139*, November 15, 1999.
36. RTCA, Environmental Conditions and Test Procedures for Airbrone Equipment, Section 8, Vibration, *RTCA Document No. RTCA/DO-160D*, December 14, 2000.
37. Viterbi, A.J., Principles of Coherent Communication, *McGraw-Hill Inc.*, 1966
38. Holmes, J.K., Coherent Spread Spectrum Systems, *John Wiley & Sons, Inc.*, 1982.
39. Simon, M.K., Omura, J.K., and et al, Spread Spectrum Communications, *Volume I, Computer Science Press*, 1985.
40. Ho., K.P., "The Effect of Interference Phase Error on Direct-Detection DPSK and DQPSK Signals," *IEEE Photonics Technology Letters, Vol. 16, No. 1*, January, 2004
41. Proakis, J.G., Digital Communications, 4th Edition, McGraw Hill, 2000.
42. Viterbi, A.J. and Omura, J.K., Principles of Digital Communication and Coding, *McGraw-Hill Inc.*, 1979
43. Franchi, A. and Harris, R.A., "On the Error Burst Properties of Viterbi Decoding," *Proc. IEEE International Conference on Communications*, pp. 1086-1091, Geneva, Switzerland, 23-26 May 1993.
44. Franchi, A. and Harris, R.A., "On the Error Burst Properties of the "Standard" K=7, Rate-1/2 Convolutional Code with Soft-Decision Viterbi Decoding," *Telecommunication Systems, Vol. 6, No. 3*, pp. 337-351, May-June 1995.
45. Porat, Y. and Reichman, A., "Burst Error Characteristics of Viterbi Decoding of Convolutional Codes," *Proc. 17th Convention of Electrical and Electronics Engineers in Israel*, pp. 230-233, Tel Aviv, Israel, 5-7 March 1991.
46. Morris, J.M., "Burst Error Statistics of Simulated Viterbi Decoded BPSK on Fading and Scintillating Channels," *IEEE Transactions on Communications, Vol. 40, No. 1*, p.34-41, January 1992
47. CCITT "Blue Book," Vol. 1, Fascicle I.3, "Terms and Definitions," *Rec.M.60, n.34, Rec.Q.9 n.0222*.
48. Nakazawa, M. and Suzuki, K., "Cesium Optical Atomic Clock: an optical pulse that tells the time," *Optics Letters, Vol. 26, No. 9*, 1 May, 2001.
49. Vig, J.R., "QUARTZ CRYSTAL RESONATORS AND OSCILLATORS, For Frequency Control and Timing Applications A Tutorial," *U.S. Army Communications-Electronics Command, Attn: AMSEL-RD-C2-PT*, Fort Monmouth, NJ 07703, USA, June 2003.